Effects of ligands on (de-)enhancement of plasmonic excitations of silver, gold and bimetallic nanoclusters: TD-DFT+TB calculations

Asadi-Aghbolaghi, Narges; Pototschnig, Johann; Jamshidi, Zahra; Visscher, Lucas

published in
Physical Chemistry Chemical Physics
2021

DOI (link to publisher)
10.1039/d1cp03220h

document version
Publisher's PDF, also known as Version of record

PCCP

ROYAL SOCIETY OF CHEMISTRY

PAPER

View Article Online
View Journal | View Issue

Cite this: *Phys. Chem. Chem. Phys.*, 2021, **23**, 17929

Effects of ligands on (de-)enhancement of plasmonic excitations of silver, gold and bimetallic nanoclusters: TD-DFT+TB calculations†

Narges Asadi-Aghbolaghi,[abc] Johann Pototschnig,[b] Zahra Jamshidi *[c] and Lucas Visscher *[b]

Received 15th July 2021,
Accepted 31st July 2021

DOI: 10.1039/d1cp03220h

rsc.li/pccp

Metal nanoclusters can be synthesized in various sizes and shapes and are typically protected with ligands to stabilize them. These ligands can also be used to tune the plasmonic properties of the clusters as the absorption spectrum of a protected cluster can be significantly altered compared to the bare cluster. In this paper, we computationally investigate the influence of thiolate ligands on the plasmonic intensity for silver, gold and alloy clusters. Using time-dependent density functional theory with tight-binding approximations, TD-DFT+TB, we show that this level of theory can reproduce the broad experimental spectra of $Au_{144}(SR)_{60}$ and $Ag_{53}Au_{91}(SR)_{60}$ (R = CH_3) compounds with satisfactory agreement. As TD-DFT+TB does not depend on atom-type parameters we were able to apply this approach on large ligand-protected clusters with various compositions. With these calculations we predict that the effect of ligands on the absorption can be a quenching as well as an enhancement. We furthermore show that it is possible to unambiguously identify the plasmonic peaks by the scaled Coulomb kernel technique and explain the influence of ligands on the intensity (de-)enhancement by analyzing the plasmonic excitations in terms of the dominant orbital contributions.

1. Introduction

In the past decade, ligand protected metal clusters with sizes ranging from 10 to a few hundred atoms have attracted attention in nanoscience due to their molecule-like properties and geometric stability. The successful synthesis and characterization of ligand protected gold,[1–6] silver[7–9] and copper[10–12] metal clusters led to extensive studies of these systems. Ligands play a significant role for the chemical and physical properties, in particular for optical properties, and provide an ideal platform for both fundamental[1,13,14] and applied[15,16] studies. The optical properties of these molecule-like structures include a wide variety of applications in the fields of electronics, catalysis, sensing, drug-delivery, bioimaging and therapy.[3,17,18]

In order to design plasmonic materials for a specific application, one of the open questions is the transition from smooth plasmonic spectra to molecular-like spectra with a number of distinct peaks. Increasing the quantum confinement for metal nanoclusters (to the range of <2 nm) produces discrete electronic structures and molecular-like excitations. The presence of ligands can reinforce this effect and also change the absorption characteristics. It has been established theoretically[14,19–22] and experimentally[12,23–25] that the enhancement and de-enhancement of the absorption spectra depends on the type of metal clusters and ligands. Modifying the ligands by changing their functional groups provides a further degree of freedom to tune the amount of charge transfer from the ligands to the cluster and thereby influence the plasmonic excitations.

A computational investigation of the effect of ligands on metal clusters is therefore timely, as for the desired applications[22,25–28] one would like to be able to predict and control their effect. For noble metal nanoclusters, various types of ligands (thiolates, phosphines, carbenes, alkynes, amine and tellurolates) can be utilized to protect them. From these possible classes of ligands, most ligand engineering studies have focused on aliphatic and aromatic thiolate ligands (with different donor and acceptor groups), as the thiol group strongly binds to gold and provides a good protection.[1,24,29,30] Depending on the size of clusters, the level of calculations used to study their electronic structure varies from detailed quantum mechanical studies,[1,31–34] to semi-classical approaches.[35,36]

The effect of ligands on the absorption spectra depends on the strength and nature of metal–ligand interactions and can be markedly different for clusters composed of different

[a] *Department of Physical Chemistry, Chemistry & Chemical Engineering Research Center of Iran, Tehran, Iran*
[b] *Division of Theoretical Chemistry, Amsterdam Center for Multiscale Modeling, Vrije Universiteit Amsterdam, The Netherlands. E-mail: l.visscher@vu.nl*
[c] *Chemistry Department, Sharif University of Technology, Tehran 11155-9516, Iran. E-mail: njamshidi@sharif.edu*

† Electronic supplementary information (ESI) available. See DOI: 10.1039/d1cp03220h

elements. Among the possible metal cores, gold and silver clusters have been intensively studied, and therefore provide a good starting point for theoretical investigations of the effects of ligands. In a previous publication,[37] some of us reported for small bare clusters the influence of scalar relativistic effects and spin–orbit coupling on the energy and intensity of plasmon-like absorption, which are especially significant for gold clusters. For gold clusters it is already established that an atomistic level of detail is important for studying its plasmonic properties. For bare silver clusters the sharp plasmonic excitation can also be well-described in a classical manner, but the situation is different for silver nanoclusters protected by a ligand where the spectra are much less sharp than in the bare clusters. For these systems it will be interesting to consider atomistic models as well.

An accurate description of plasmons including the detailed quantum nature of excitations is challenging. In particular variants of time-dependent density functional theory are used to calculate absorption spectra of (bare) gold and silver nanoparticles,[38–52] and detailed discussions of the efficiency and limitations of these approaches are available in literature.[53–57] Among these, the traditional ''Casida-type'' TD-DFT formalism is used extensively for small ligand-protected clusters and has a computational cost depending on, and increasing rapidly with, the number of exited-states that need to be determined. An alternative is real-time propagation, which also has been used for the absorption spectrum of the large clusters (more than 100 atoms) protected with ligands.[58–60] While providing similar or higher accuracy than Casida-type TD-DFT, it is more difficult in real-time DFT to analyze the nature of states in terms of orbital contributions, which is why we focus on Casida-type TD-DFT in the current work.

In our previous work,[37,55] we introduced TD-DFT+TB as a fast and efficient approach to investigate plasmonic excitations of systems with a number of states ranging from 3000 to 30 000. The key advantage over the still faster time-dependent tight binding density functional (TD-DFTB), is the fact that the tight-binding approximation is applied only after the DFT ground state calculation, thereby avoiding the need for explicit parameterization. A related method is the TDDFT-as approach of Della Sala and coworkers, who have shown that reducing the auxiliary basis in TD-DFT to just one function can yield a very accurate description of plasmonic excitations for silver nanoparticles at a greatly reduced cost relative to a full TD-DFT calculation.[41,57]

For the application to ligand-protected nanoclusters, the TD-DFT+TB method (being based on Kohn–Sham orbitals) has the advantage that the splitting of plasmonic excitations can be analyzed in terms of Kohn–Sham single-orbital transitions. In this work we exploit this feature by analyzing the plasmonic excitations of monometallic gold, silver, as well as bimetallic nanoclusters (with 20, 56, 120, 144 atoms) protected by thiolate SCH_3 and SC_6H_6 ligands. The change of s- and d-orbital contributions to the Kohn–Sham transitions relative to those in the bare clusters explains the (de-)enhancement of intensity and can be modified by changing the type and functionalization of the ligands.

2. Computational details

We apply the TD-DFT+TB method as described in ref. 30 and implemented in the ADF2019.1 package.[61] Following previous experimental and theoretical work we focus on thiolate ligands (SCH_3 and SC_6H_5).[3,14,29,62–64] For the metal nanoclusters we consider tetrahedral structures with 20, 56 and 120 atoms, as well as clusters with 144-atoms which were found to be very stable experimentally.[65–67] We define the overall charge of the clusters such that the electronic ground state of the studied systems can be taken as closed shell. Optimized structures of the ligated clusters were obtained in the local density approximation (LDA) of the exchange–correlation (*xc*) functional,[68] with a double-zeta (DZ) slater type basis set. The absorption spectra of the clusters with and without ligands were calculated (in the range of 0.0–6.0 eV) with the asymptotically corrected LB94 *xc*-functional in the scalar relativistic zeroth-order regular approximation (ZORA) to the Dirac Hamiltonian.[69,70] The LB94 model potential typically gives good absorption spectra,[45,47,71–73] and has been shown[74] to agree reasonably well with long-range corrected hybrid functionals for Ag_{20}. Plasmonic excitations under the influence of ligands were analyzed by determining the atomic orbital contribution on the excitations. To distinguish the collective plasmonic excitation from the single-particle excitations, the Coulomb-kernel-scaling method of Bernadotte *et al.*[75] was applied.

3. Results and discussion

3.1 The effect of ligands on the plasmon excitations of monometallic Au and Ag nanoclusters

In this section, we discuss the effect ligands have on the absorption spectra of monometallic nanoclusters. We will only consider TD-DFT+TB absorption spectra in the following, but provide for the smallest clusters ($Ag_{20}SCH_3$ and $Au_{20}SCH_3$) also a comparison with the more expensive TD-DFT as well as the cheaper TD-DFTB approaches in the ESI† (Fig. S1). This data supports the conclusion of our previous work[37,55] that TD-DFT+TB can be used as a replacement for TD-DFT in studies of metallic nanoclusters. The tetrahedral structures for gold and silver nanoclusters can be defined for 20, 56 and 120 atoms, and these structures are good models for studying surface enhance Raman spectroscopic (SERS) and single molecule detection. We note that the tetrahedral 20 atom models with a single adsorbed molecule do not present the lowest-energy structural isomers and should be considered as model systems. Experimental data typically refers to larger, fully ligand-protected, systems that have more pronounced plasmonic excitations. We merely chose these models for ease of comparison with the larger tetrahedral clusters considered later.

In Fig. 1a and b we display how adding just one thiolate SCH_3 or SC_6H_5 ligand can already alter the sharp high-intensity peak of these nanoclusters. The strength of the thiolate ligand binding depends on electron affinity of the metal cluster and especially gold clusters, which have a higher affinity than their silver counterparts, have extraordinary stability when thiol-protected. The effect of the ligand on the two types of clusters is markedly different, with a splitting and decrease of intensity of sharp plasmonic excitations for silver

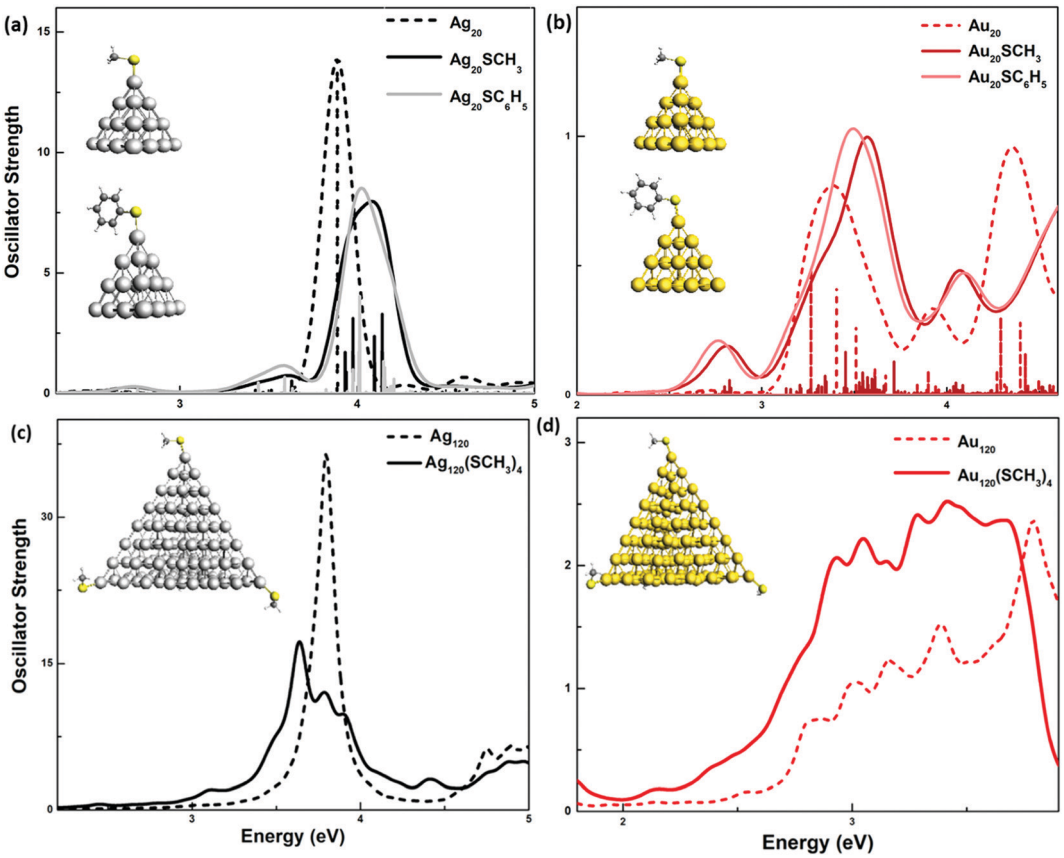

Fig. 1 Calculated TD-DFT+TB absorption spectra for (a and b) $Ag_{20}SCH_3(SC_6H_5)$ and $Au_{20}SCH_3(SC_6H_5)$ and (c and d) $Ag_{120}(SCH_3)_4$ and $Au_{120}(SCH_3)_4$ in comparison to bare clusters. Spectra have been broadened with a σ = 0.2 eV Gaussian.

(Fig. 1a) while the much broader plasmon-like excitations appear to be somewhat enhanced for gold (Fig. 1b). For both elements, the excitation energies are shifted to the blue compared to the bare clusters. This behavior does not depend on the functional group (alkyl or phenyl) of the thiol. We furthermore note at low energy (2–3 eV) charge-transfer ligand-to-metal excitations.

Fig. 1 also contains the absorption spectra of the larger clusters, Ag_{120} and Au_{120}, to which we add four ligands. Fig. 1c and d reveal the same trend for $Ag_{120}(SCH_3)_4$ and $Au_{120}(SCH_3)_4$ as the smaller ones. By adding four SCH_3 ligands, the sharp high-intensity peaks of Ag_{120} (around 3.0–4.0 eV) are quenched and the broad low-intensity plasmonic excitations of Au_{120} (at 2.5–3.5 eV) are clearly enhanced. The effect on peak positions is less clear as the dominant peak is split in the $(SCH_3)_4$ case and also shifts differently when applying an alkyl or a phenyl group (see Fig. S2 (ESI†) for 56-atomic clusters). In the ESI† we furthermore provide absorption spectra of highly protected metal clusters with SC_6H_5 ligands,[76,77] $Ag_{30}(SC_6H_5)_{18}$ and $Au_{30}(SC_6H_5)_{18}$. As can be seen in Fig. S3 (ESI†), they exhibit a similar trend with ligand adsorption: de-enhancing and enhancing for silver and gold, respectively.

3.2 The effect of ligands on the plasmon excitations of bimetallic AgAu nanoclusters

The different optical behavior of pure gold and silver clusters make the tailoring of these properties by creating bimetallic alloys an interesting topic of research. From previous work,[37,55] it emerges that the chemical composition of clusters has a large influence on the intensity and energy of plasmon peaks. It has been well established[37] that alloying gold by silver reduces the d-character of excitations and increases the s-character, thereby making these more plasmonic. In this section we consider the additional effect of ligands on the optical properties. Fig. 2 shows the absorption spectra of 20- and 120-atom bimetallic structures with a single and with four SCH_3 ligands (results for SC_6H_5 are shown in the ESI,† in Fig. S4).

For $Ag_{16}Au_4SCH_3$ in Fig. 2a, the intensity of plasmonic transitions decreases and their energies are shifted to the blue with respect to bare clusters. For this complex the high ratio of Ag atoms leads to a plasmonic absorption reminiscent of that of pure $Ag_{20}SCH_3$, but with the quenching of the (already lower) plasmonic peak being less prominent than for Ag_{20}. For the opposite composition, Ag_4Au_{16}, the change in the spectrum differs from that of pure Au_{20} with the interaction of ligands not clearly enhancing (nor quenching) the peaks in the range of 3.0 to 4.0 eV. One aspect to consider is whether the anchoring of the thiol to either a silver atom (Ag_{20} and Ag_4Au_{16}) or to a gold atom (Au_{20} and Ag_4Ag_{16}) is of importance. This appears to be of minor importance, the strength of thiol–gold bond (and the amount of transferred charge) in the $Ag_{16}Au_4SCH_3$ complex equals $\Delta E_b = -2.9$ eV($|\Delta q| = 0.74$), while the silver–thiol bond in

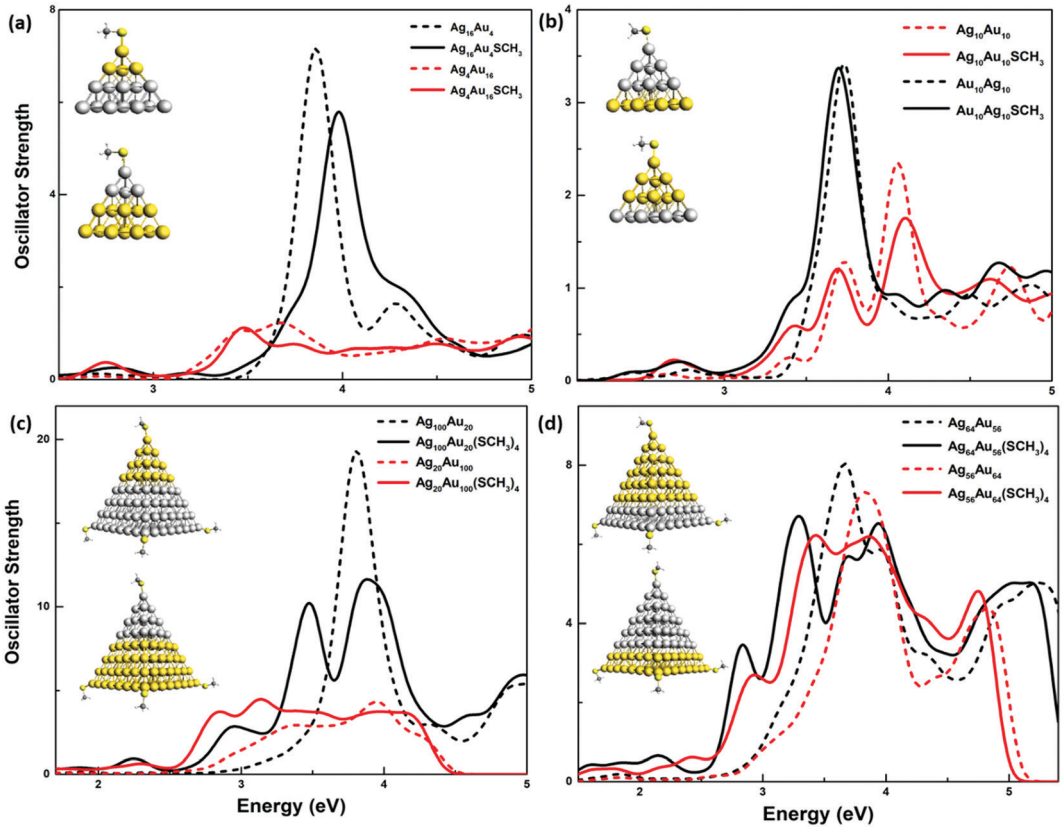

Fig. 2 Calculated TD-DFT+TB absorption spectra for (a) $Ag_{16}Au_4SCH_3$ and $Ag_4Au_{16}SCH_3$ (b) $Ag_{10}Au_{10}SCH_3$ and $Au_{10}Ag_{10}SCH_3$. (c) $Ag_{100}Au_{20}(SCH_3)_4$ and $Ag_{20}Au_{100}(SCH_3)_4$ (d) $Ag_{65}Au_{56}(SCH_3)_4$ and $Ag_{56}Au_{64}(SCH_3)_4$. Spectra have been broadened with a σ = 0.2 eV Gaussian.

$Au_{16}Ag_4SCH_3$ has $\Delta E_b = -3.0$ eV($|\Delta q| = 0.67$). The strength of the metal–ligand bond in the bimetallic clusters is thus smaller than in the monometallic gold cluster (see Table S1, ESI†).

For the larger tetrahedral clusters, $Ag_{100}Au_{20}$ and $Ag_{20}Au_{100}$, the absorption spectra (see Fig. 2c) under the influence of four thiolates show the same qualitative characteristics as for the smaller clusters: a marked quenching for the silver-dominated $Ag_{100}Au_{20}$ cluster and a small enhancement for the gold-dominated $Ag_{20}Au_{100}$ cluster. For clusters with the same ratio of Ag and Au atoms ($Ag_{10}Au_{10}$ and $Au_{10}Ag_{10}$) the situation is less clear. We see almost no effect of the ligand for the silver-bound $Ag_{10}Au_{10}$, while for the gold-bound $Au_{10}Ag_{10}$ a quenching of the peak at 4.2 eV is visible in Fig. 2b. For the larger clusters, $Ag_{64}Au_{56}(SCH_3)_4$ and $Ag_{56}Au_{64}(SCH_3)_4$, with nearly the same ratio of Ag and Au atoms, Fig. 2d does not reveal a clear trend. Since the effect of ligands was observed to be opposite for pure gold and pure silver clusters in the preceding section, this is perhaps intuitively what would be expected for clusters with the same ratio of gold and silver atoms. To provide more insight in the precise mechanism of enhancement or quenching, we consider in more detail the orbital nature of these plasmonic excitations in the next section. We will, however, first consider the available experimental data for bimetallic clusters and compare this with our calculated spectra.

The absorption spectra of the nanoalloys $(AgAu)_{144}(SR)_{60}$ were first observed by electrospray ionization mass spectrometry by Kumara and Dass.[20,78] These fascinating structures have since then attracted much attention as the synthesis process allows for varying the metal composition of the cluster.[20,79–81] The comparison of these fully ligated clusters with the bare clusters then provides valuable insight on how the metal plasmonic response is influenced by the ligand protection.[22,49,82,83] Fig. 3 displays the absorption spectra for ligand protected nanoalloys with different ratios of Au and Ag atoms and also shows the effect of ligand on pure isolated grand core 114-atomic and *ad hoc* 144-atomic clusters. The $Au_{144}(SCH_3)_{60}$ cluster consists of 114 Au core atoms with a 30-unit protective layer of $Au(I)–(SCH_3)_2$. The same structure can be made with a silver core, yielding $Ag_{144}(SCH_3)_{60}$. By increasing the number of atoms from 114 to 144 atoms, the intensity of the plasmon excitations is enhanced for both types of clusters. The monolayer of SCH_3 groups clearly reduces the intensity of sharp plasmonic peaks of Ag_{144} in the range of 3.5–4.5 eV (in Fig. 3a). However, for $Au_{144}(SCH_3)_{60}$ (in Fig. 3b), the absorption peaks below 3.0 eV are intensified, while for the higher energy range (>3.0 eV) the intensities are almost the same as for bare Au_{144}. We thus see the same general trend as discussed before for the tetrahedral monometallic clusters. Turning to the bimetallic cores, Fig. S5 (ESI†) displays the spectrum of an icosahedral core–shell $Ag_{91}Au_{53}(SCH_3)_{60}$ (with an Au core and an Ag shell) in comparison to the bare $Ag_{91}Au_{53}$ cluster and has the same quenching and broadening of absorption spectra as visible in Ag-dominated clusters. On the other hand, for $Ag_{53}Au_{91}(SCH_3)_{60}$

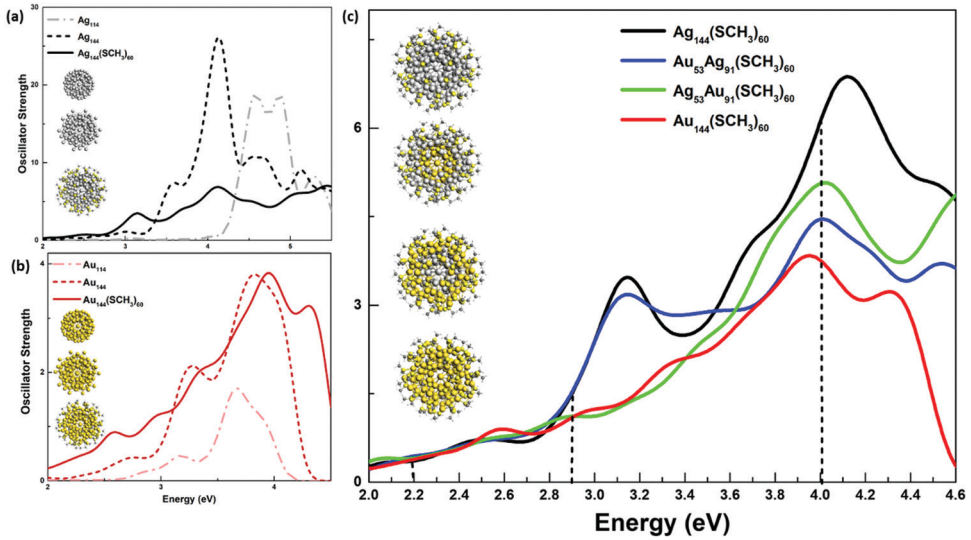

Fig. 3 Calculated TD-DFT+TB absorption spectra for (a and b) pure grand core 114-atomic and *ad hoc* 144-atomic structures of silver and gold with and without SCH_3 ligand (c) $Ag_{144}(SCH_3)_{60}$, $Au_{144}(SCH_3)_{60}$, $Ag_{53}Ag_{91}(SCH_3)_{60}$, and $Au_{53}Ag_{91}(SCH_3)_{60}$. The dashed lines indicate the experimental peaks for $Au_{144-X}Ag_X(SR)_{60}$ from ref. 20. Spectra have been broadened with a σ = 0.2 eV Gaussian.

(with an Ag core and Au shell) we see an enhancement of the absorption intensity compared to the bare cluster (for energies below 4 eV). This can be explained with the larger amount of gold with respect to the silver and the anchoring of SCH_3 with the gold atoms (see the structures depicted in Fig. S5, ESI†).

Turning back to Fig. 3 we will now compare to experimental data. The experimental absorption spectra, for $Au_{144-X}Ag_X(SR)_{60}$ clusters exhibit three peaks around 560 (2.2 eV), 430 (2.9 eV) and 310 nm (4.0 eV), which are more distinct for a high ratio of silver.[20,81,84] The spectra of $Ag_{53}Au_{91}(SCH_3)_{60}$ and $Au_{53}Ag_{91}(SCH_3)_{60}$ in comparison to the pure $Au_{144}(SCH_3)_{60}$, $Ag_{144}(SCH_3)_{60}$ are available in Fig. 3. For all of these clusters we observe, in agreement with experiment, the high intensity peak around 4 eV, which is intensified by going from $Au_{144}(SCH_3)_{60}$ to the bimetallic cluster. It has been well established that for bare bimetallic clusters, increasing the ratio of Ag enhances the plasmonic absorption. For the peak at 4 eV the higher intensity of $Ag_{53}Au_{91}(SCH_3)_{60}$ in comparison to $Au_{53}Ag_{91}(SCH_3)_{60}$ exhibits, however, the differential effect of thiolate ligands bounded to Au and/or Ag shell as the relatively strongest absorption is for the cluster with the smallest Ag/Au ration. This is not the case for the lower excitation around 3 eV, where the intensity of $Au_{53}Ag_{91}(SCH_3)_{60}$ is similar to that of $Ag_{144}(SCH_3)_6$. As mentioned before, these low energy excitations (3.0–3.3 eV) are dominated by thiol-to-metal charge-transfer excitations (about 70–77%). This could explain the similarity of this peak in clusters that have the same outer layer.

3.3 The effect of ligand functional groups on the plasmon excitations

Chemical modification (functionalization) of ligands can be employed to change spectral features as energy positions and intensities. In experimental work, thiolate ligands (–SR) nanocluster with various functional groups (R) have been synthesized and used to tune plasmonic properties.[24,25,63,76] To connect to such approaches, we look in this section at the influence of electron donor (–CH_3, –^{t}Bu and –OH) and electron acceptor (SCH_2COOH, –COOH, and –NO_2) functional groups on the plasmonic excitations of ligand-protected Au_{20} and Ag_{20}. The effect of functional groups on alkyl and phenyl thiolate ligands are displayed in Fig. 4. For the alkyl ligands, substituting the electron donating and accepting R-groups does not result in significant changes in the plasmon peaks of $Ag_{20}SCH_3$ and $Au_{20}SCH_3$ complexes. For aromatic ligands, the electron donation takes place from the phenyl to the metal cluster. For the main plasmon excitations of Ag_{20}, around 4 eV, the effect of altering the functional groups is again almost negligible and the quenching of the plasmonic peak remains the same as for unsubstituted $Ag_{20}SC_6H_5$. For the gold clusters, however, the spectra are clearly dependent on the choice of ligand functional groups. This is in agreement with Clays *et al.*[30] who found the effects of R-group on the geometrical structures of Au_{20} to be insignificant, but pointed out the influence of this group on the energies of the HOMO, LUMO and other valence orbitals relevant for the spectra. For the main plasmon excitations of $Au_{20}SC_6H_5$, the intensity decreases by substitution of electron withdrawing R-groups and slightly increases for the electron donating R-groups (see Fig. 4d).

The effect of varying the functional group is more obvious in the low-energy ligand-to-metal transitions, between 2 to 3 eV, see ESI.† The high intensity peaks, in this range of energy are, however, typically charge-transfer (CT) excitations (see Fig. S6, ESI†) and are thus less well described by the LB94 model potential which lacks exact exchange. A more adequate description is provided by non-local range-separated hybrid,[85] which is unfortunately difficult to combine with the tight-binding approximation that we use here. Noting these uncertainties in the precise location of the low-energy peaks, we will in the following section discuss the enhancement or quenching of excitations by analyzing their orbital contributions.

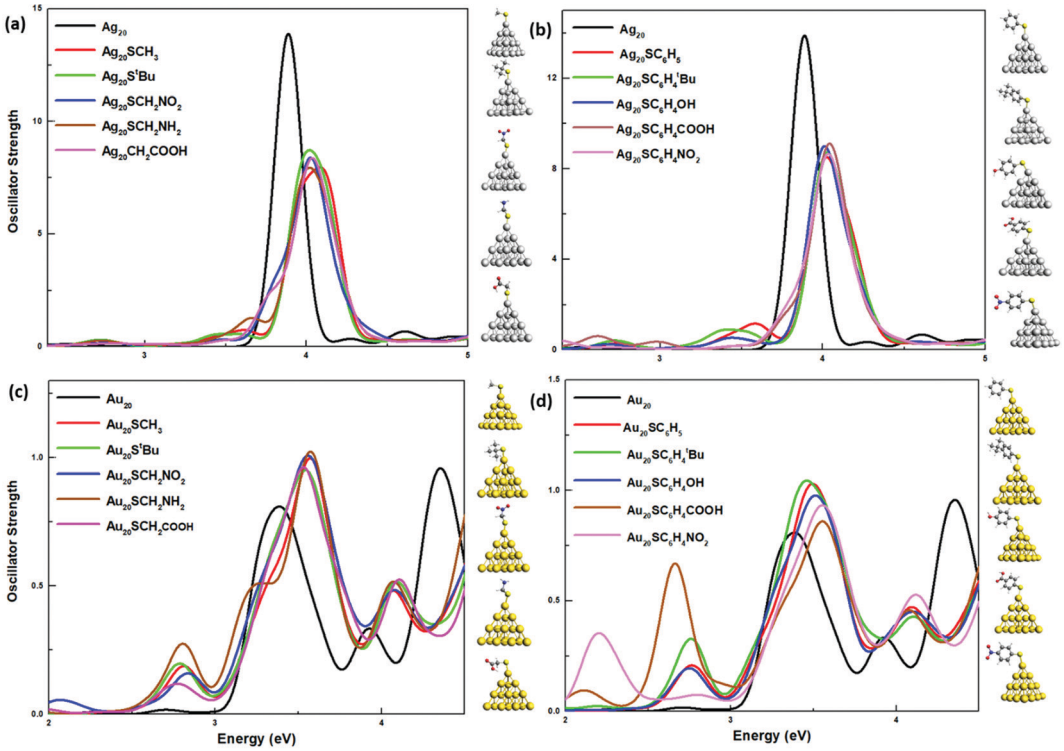

Fig. 4 Calculated TD-DFT+TB absorption spectra for Ag_{20} (a and b) and Au_{20} (c and d) with different donor and acceptor functional groups. Spectra have been broadened with a σ = 0.2 eV Gaussian.

3.4 Orbital contributions analysis

The analysis of electronic structure and contribution of the orbitals can be helpful to understand the observed variations of intensity. Table 1 reports the percentage of atomic d- and sp-character to the plasmonic excitations using the following equation;[86]

$$\%i = \frac{\sum_{n}^{\Omega_n < E_c} f_n \sum_{ov} |F_n^{ov}|^2 |\langle i|\phi_o\rangle|^2}{\sum_{n}^{\Omega_n < E_c} f_n} \times 100 \qquad (1)$$

where i denotes an atomic orbital with d- or sp-character, $\langle i|\phi_o\rangle$ is its projection on the occupied orbitals $|\phi_o\rangle$, f_n is the oscillator strength of the excitation at energy Ω_n, and $|F_n^{ov}|^2$ is the weight of a particular single orbital transition from an occupied (o) to a virtual (v) orbital in this transition. All transitions are weighted by their oscillator strengths, f_n, and summed over all transitions up to a certain energy cut off E_c (the range of energy differs for each type of clusters). The equivalent summation over oscillator strengths in denominator serves as a normalization factor.

In Table 1 the quenching of oscillator-strength for the high intensity excitations of Ag_{20} in the presence of ligands is listed for the range of 3.30 to 4.60 eV. This quenching is caused by the screening of s-electrons of silver that is visible as a decrease in the sp-contribution percentage from 100% to 61–66%. For bare nanoclusters, this corroborates with the well-established notion that reduction of s-character by increased participation of d-electrons in the plasmonic transitions quenches them and broadens the spectrum.[37] However, for ligated clusters the screening of s-electrons of Ag is not due to d-electrons as the contribution of d-electrons remains almost constant at less than 0.1%. Instead, the splitting of the sharp peaks of Ag_{20} is now due to the participation of the ligand s- and p-orbitals that contribute with a weight of 34–39% (Table 1). For Au_{20}, the

Table 1 Percentage of orbital-contributions for the high-intensity plasmonic transitions[a] showing the effect of ligands

Structures	d-Au	d-Ag	sp-Au	sp-Ag	sp-ligand
Ag_{20}	—	0.0	—	100.0	—
$Ag_{20}SCH_3$	—	0.06	—	65.6	34.3
$Ag_{20}SC_6H_5$	—	0.02	—	61.2	38.7
Ag_{144}	—	12.4	—	87.6	—
$Ag_{144}(SCH_3)_{60}$	—	3.7	—	14.6	81.7
Au_{20}	88.2	—	11.8	—	—
$Au_{20}SCH_3$	72.7	—	19.3	—	8.0
$Au_{20}SC_6H_5$	57.9	—	20.8	—	21.2
Au_{144}	94.5	—	5.5	—	—
$Au_{144}(SCH_3)_{60}$	41.0	—	12.7	—	46.2
$Ag_{16}Au_4$	46.3	0.05	9.3	44.4	—
$Ag_{16}Au_4SCH_3$	54.9	0.14	7.7	17.3	19.9
$Ag_{91}Au_{53}$	56.2	8.5	12.2	23.1	—
$Ag_{91}Au_{53}(SCH_3)_{60}$	30.4	2.3	10.8	1.9	54.6
Ag_4Au_{16}	78.3	—	13.9	7.8	—
$Ag_4Au_{16}SCH_3$	52.6	0.15	19.6	9.6	18.1
$Ag_{53}Au_{91}$	90.6	0.03	8.6	0.8	—
$Ag_{53}Au_{91}(SCH_3)_{60}$	26.2	0.00	11.9	4.2	57.6

[a] Excitations in the range of 2.5–5.0 eV.

participation of ligand orbitals is also important, but here the effect on the plasmonic excitation is opposite. The electrons of ligands now screen the d-electrons of gold and give rise to higher oscillator strengths than for the pure d-transitions. The d-contribution, which is 88% for isolated Au_{20}, decreases to 73% and 58% for $Au_{20}SCH_3$ and $Au_{20}SC_6H_5$, respectively (Table 1). These opposing effects of ligands on gold and silver transitions result in changes of the intensity upon ligation that are overall smaller for the bimetallic clusters than for the pure clusters. In Table 1, the sp-orbital contributions of silver for $Ag_{16}Au_4$ are about 44%, clearly less than for pure Ag_{20} (100%), and this contribution decreases to 17%, upon interaction with ligands in $Ag_{16}Au_4SCH_3$. At the same time, the already large d-contribution of gold further increases from 46% to 55%, which is different from the effect of ligand coating on a pure gold cluster.

The analysis of orbital-contributions for pure and alloy 144-atomic clusters confirms the trends seen in the smaller pure metal clusters. As listed in Table 1, for Ag_{144} and Au_{144}, after coating with ligands the s-electrons and d-electrons are screened, resulting in quenching and enhancing of intensity, respectively (Fig. 3). For the $Ag_{91}Au_{53}$ and $Ag_{53}Au_{91}$ bimetallic clusters, the variation of orbital contributions roughly follows the trend of the metal with the higher ratio. Ligand coating leads for $Ag_{91}Au_{53}$ to a decrease of the s-contribution of silver from 23% to 2% and a decrease of the d-character of gold from 56% to 30%. For $Ag_{53}Au_{91}$, the d-contribution of gold decreases from 91% to 26% (and the silver s-character changes slightly from 1% to 4%).

The orbital-contribution analysis can be complemented by looking at the partial density of state (pDOS) shown in Fig. 5. The pDOS clearly shows a decrease in of s-electron density for silver near the Fermi level. For gold the interaction with ligands pushes the d-levels further below the Fermi level and thereby diminishes the density of d-electrons in excitations. This reduction of d-partial density of states by adding ligands was also observed by López-Lozano *et al.*[83] Moreover, the availability of s-orbitals of ligands with higher energies can explain the blue-shift of absorption spectra observed in Fig. 1. For gold clusters, the participation of d-orbitals in plasmon excitations is reduced by increasing the size.[37] This makes the effect of ligands for the larger $Au_{120}(SCH_3)_4$ structure (Fig. 5d) less pronounced than for the smaller cluster.[83] The same holds for the sp-DOS for $Ag_{120}(SCH_3)_4$ which shows a relatively smaller effect compared to the bare Ag_{120} cluster.

For these highly symmetric clusters, an additional effect of ligand coating is a reduction of symmetry which splits the excitation energy levels and thus broadens the spectra. For instance, the high-intensity peak of Ag_{20} consists of a number of degenerate transitions at 3.89 eV with a summed oscillator

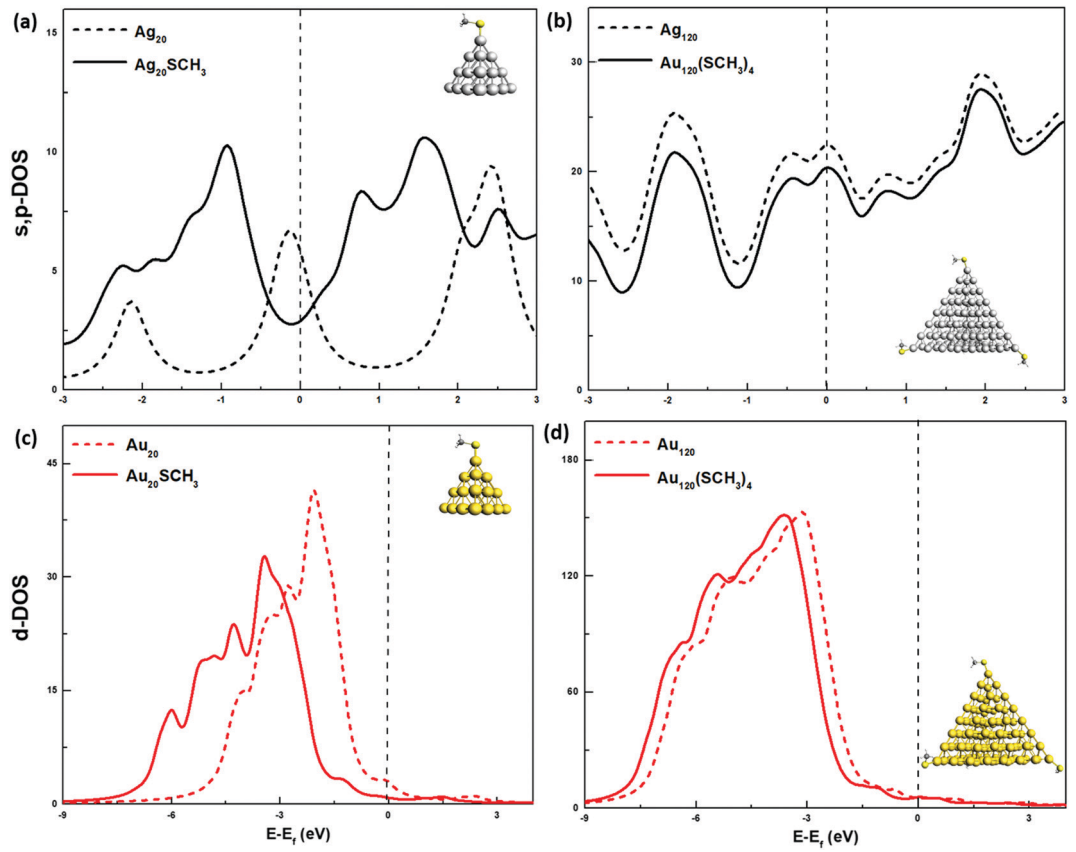

Fig. 5 Partial density of state (a and b) s,p-DOS of $Ag_{20}SCH_3$ and $Ag_{120}(SCH_3)_4$, and (c and d) d-DOS of $Au_{20}SCH_3$ and $Au_{120}(SCH_3)_4$ in comparison to bare clusters.

strength f = 13.89, and is split into six or seven non-degenerate transitions (with energies between 3.93 to 4.14 eV) after interaction with ligands. The total summed oscillator strength of these transitions is f = 12.73 (see Table S2, ESI†). The effect of symmetry-breaking can also be considered by looking at the range of orbitals (HOMO to HOMO−5) contributing to this main Ag_{20} peak. For the bare cluster these orbitals are split by about 0.27 eV while for $Ag_{20}SCH_3$ ($Ag_{20}SC_6H_5$) this energy range increases to 0.52 (0.59) eV (see ESI,† Fig. S7). For $Au_{20}SCH_3(SC_6H_5)$, the change in d- and s-contributions is probably more important than the reduction of symmetry. For the bare Au_{20} cluster, no high-intensity degenerate peaks (in range 3–4 eV) are found and the summed oscillator strength is modest at is f =1.81. As can be seen in Table S3 (ESI†) this sum increases to 1.94 after interaction with ligands. The orbital energy range is at the same time broadened from about 0.39 eV for Au_{20} to 0.66 (0.67) eV for $Au_{20}SCH_3$ ($Au_{20}SC_6H_5$) (see ESI,† Fig. S7).

3.5 Coulomb kernel scaling

In previous sections, for both silver and gold an overall broadening of the absorption spectrum under the effect of ligands is observed. This broadening makes it harder to recognize the plasmonic peaks for ligand-protected clusters than for bare clusters. One possibility is to use visualization, Gieseking *et al.*[87] implemented an analytical tool to identify plasmon-like excitations by plotting characteristic features of plasmonic excitations (large superatomic extent, collectivity and dipole additivity) relative to other type of excitations.

An alternative is the Coulomb-scaling technique introduced by Bernadotte *et al.*[53] This analysis of plasmon transitions is based on the fact that the plasmonic excitation responds much more strongly to a scaling of the Coulomb kernel than other excitations. We will focus on the ligand-coated 144-atoms clusters as these are highly stable and well characterized experimentally. Fig. 6 compares the absorption spectra of $Au_{144}(SR)_{60}$ and $Ag_{\sim 53}Au_{\sim 91}(SR)_{60}$ recorded by Dass *et al.*[20] to the computed TD-DFT+TB spectra of $Au_{144}(SCH_3)_{60}$ and $Ag_{53}Au_{91}(SCH_3)_{60}$. For both pure and alloy clusters, the overall shapes of the computed spectra are in good agreement with experiment, but it is hard to locate the plasmonic excitations. To identify these transitions, we scaled the Coulomb kernel from the noninteracting limit (λ = 0) to the fully interacting limit (λ = 1) by steps of 0.2 and plotted the resulting variation of excitation energies in the range of 1.50 and 3.00 eV as a function of λ. The λ-dependency of the excitation energies in the vicinity of the most intense peaks of the experiment, 560 (2.2 eV) and 430 nm (2.9 eV) for $Ag_{\sim 53}Au_{\sim 91}(SR)_{60}$ and 520 nm (2.4 eV) for $Au_{144}(SR)_{60}$ (indicated by dashed lines) can thus be studied. Fig. 6c and d show a strong λ-dependency of the excitation at 2.90 eV for $Au_{91}Ag_{53}(SCH_3)_{60}$ and for $Au_{144}(SCH_3)_{60}$ at 2.40 and 2.61 eV, that demonstrates their plasmonic nature. In the lower energy range, excitations at 2.06 and 1.60 eV for $Au_{91}Ag_{53}(SCH_3)_{60}$ and $Au_{144}(SCH_3)_{60}$,

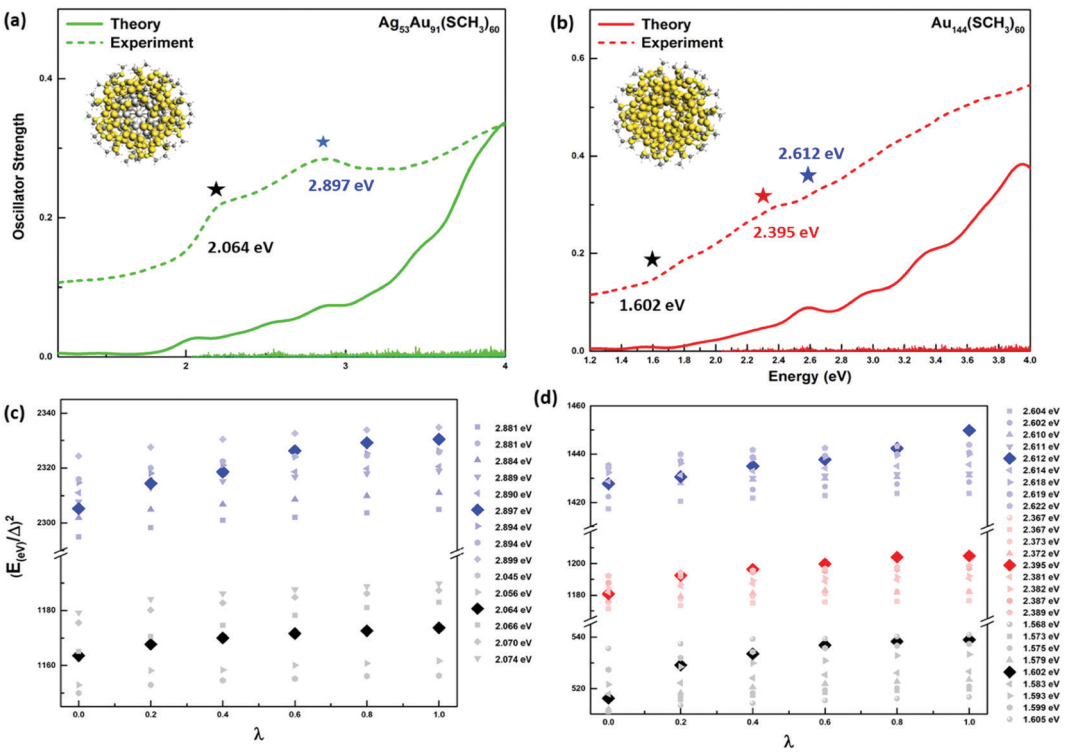

Fig. 6 Calculated TD-DFT+TB absorption spectra for (a) $Ag_{53}Au_{91}(SCH_3)_{60}$ and (b) $Au_{144}(SCH_3)_{60}$ in comparison to experimental spectra from ref. 20 for $Ag_{53}Au_{91}(SR)_{60}$ and $Au_{144}(SR)_{60}$. Spectra have been broadened with a σ = 0.2 eV Gaussian. The variation of the squared excitation energies for high-intensity peaks of (c) $Ag_{53}Au_{91}(SCH_3)_{60}$ and (d) $Au_{144}(SCH_3)_{60}$ upon scaling the electronic interaction with excitation energies being plotted separately in units of the HOMO–LUMO gap Δ.

respectively, can also be identified as plasmonic excitations although their λ-dependency is weaker than found in the high energy range.

4. Conclusion

Plasmonic excitations of metal nanoclusters are shown to be affected by the addition of protective ligands. The effect of these ligands depends on the element used for the core, for silver nanoclusters a quenching and broadening of sharp plasmonic excitation is seen, while we observe an increase in the absorption intensities for gold cores. The effect of size, composition and ligand functionalization on large cluster models can be studied in full atomistic detail with the TD-DFT+TB method. The ensuing orbital contribution analysis can thereby explain the enhancing and quenching effects of ligands on gold and silver, respectively, in terms of screening of the d-electrons of gold and s-electrons of silver by the sp-ligand orbitals. For the stable nanoclusters, $Au_{144}(SR)_{60}$ and $Au_{91}Ag_{53}(SR)_{60}$, we observe good agreement of the computed TD-DFT+TB spectra with the experimental observations. For these cases we also demonstrated that it is possible to discriminate the plasmonic excitations from the single particle excitations by the Coulomb kernel scaling technique. The economical TD-DFT+TB approach thereby provides a versatile tool to analyze and predict the effect of ligand coating on plasmonic nanoalloys.

Conflicts of interest

There are no conflicts to declare.

Acknowledgements

We acknowledge the developer group of Software for Chemistry & Materials (SCM) and computing resources of VU University of Amsterdam. We would like to thank Prof. A. Dass for sharing the experimental data. N. A. acknowledges financial support from Student Affair of Ministry of Science and Technology of Iran. J. P. acknowledges funding by the Austrian Science Fund (FWF):J 4177-N36. Z. J. acknowledges the Holland Research School for Molecular Chemistry for a fellowship.

References

1 R. Jin, *Nanoscale*, 2015, **7**, 1549–1565.
2 X. Kang, H. Chong and M. Zhu, *Nanoscale*, 2018, **10**, 10758–10834.
3 Y. Chen, J. Wang, C. Liu, Z. Li and G. Li, *Nanoscale*, 2016, **8**, 10059–10065.
4 A. Das, T. Li, G. Li, K. Nobusada, C. Zeng, N. L. Rosi and R. Jin, *Nanoscale*, 2014, **6**, 6458–6462.
5 N. A. Sakthivel, S. Theivendran, V. Ganeshraj, A. G. Oliver and A. Dass, *J. Am. Chem. Soc.*, 2017, **139**, 15450–15459.
6 R. Jin, *Nanoscale*, 2010, **2**, 343–362.
7 M. J. Alhilaly, M. S. Bootharaju, C. P. Joshi, T. M. Besong, A.-H. Emwas, R. Juarez-Mosqueda, S. Kaappa, S. Malola, K. Adil and A. Shkurenko, *J. Am. Chem. Soc.*, 2016, **138**, 14727–14732.
8 N. Cathcart, P. Mistry, C. Makra, B. Pietrobon, N. Coombs, M. Jelokhani-Niaraki and V. Kitaev, *Langmuir*, 2009, **25**, 5840–5846.
9 Z. Wu, E. Lanni, W. Chen, M. E. Bier, D. Ly and R. Jin, *J. Am. Chem. Soc.*, 2009, **131**, 16672–16674.
10 A. Baghdasaryan, C. Besnard, L. M. Lawson Daku, T. Delgado and T. Burgi, *Inorg. Chem.*, 2020, **59**, 2200–2208.
11 A. Ganguly, I. Chakraborty, T. Udayabhaskararao and T. Pradeep, *J. Nanopart. Res.*, 2013, **15**, 1522–1528.
12 Z. Wang, B. Chen and A. L. Rogach, *Nanoscale Horiz.*, 2017, **2**, 135–146.
13 M. Shabaninezhad, A. Abuhagr, N. A. Sakthivel, C. Kumara, A. Dass, K. Kwak, K. Pyo, D. Lee and G. Ramakrishna, *J. Phys. Chem. C*, 2019, **123**, 13344–13353.
14 L. Sementa, G. Barcaro, A. Dass, M. Stener and A. Fortunelli, *Chem. Commun.*, 2015, **51**, 7935–7938.
15 J. Lifeng, H. Tao, L. Zhipeng and L. Xue-Mei, *Chin. J. Catal.*, 2010, **31**, 1307–1315.
16 M. Aslam, N. Chaki, J. Sharma and K. Vijayamohanan, *Curr. Appl. Phys.*, 2003, **3**, 115–127.
17 P. Wang, Z. Lin, X. Su and Z. Tang, *Nano Today*, 2017, **12**, 64–97.
18 P. D. Howes, R. Chandrawati and M. M. Stevens, *Science*, 2014, **346**, 1247390.
19 G. U. Kuda-Singappulige and C. M. Aikens, *J. Phys. Chem. A*, 2019, **123**, 9712–9720.
20 C. Kumara and A. Dass, *Nanoscale*, 2011, **3**, 3064–3067.
21 R. D. Senanayake and C. M. Aikens, *Phys. Chem. Chem. Phys.*, 2020, **22**, 5272–5285.
22 S. Malola, L. Lehtovaara, J. Enkovaara and H. Häkkinen, *ACS Nano*, 2013, **7**, 10263–10270.
23 R. Bauld, M. Hesari, M. S. Workentin and G. Fanchini, *Nanoscale*, 2014, **6**, 7570–7575.
24 R. R. Nasaruddin, T. Chen, N. Yan and J. Xie, *Coord. Chem. Rev.*, 2018, **368**, 60–79.
25 X. Yuan, N. Goswami, W. Chen, Q. Yao and J. Xie, *Chem. Commun.*, 2016, **52**, 5234–5237.
26 S. K. Ghosh, S. Nath, S. Kundu, K. Esumi and T. Pal, *J. Phys. Chem. B*, 2004, **108**, 13963–13971.
27 A. Cirri, H. Morales Hernández, C. Kmiotek and C. J. Johnson, *Angew. Chem., Int. Ed.*, 2019, **58**, 13818–13822.
28 S. Pocoví-Martínez, M. Parreno-Romero, S. Agouram and J. Pérez-Prieto, *Langmuir*, 2011, **27**, 5234–5241.
29 J. Jung, S. Kang and Y.-K. Han, *Nanoscale*, 2012, **4**, 4206–4210.
30 S. Knoppe, H. Häkkinen, T. Verbiest and K. Clays, *J. Phys. Chem. C*, 2018, **122**, 4019–4028.
31 R. Rüger, E. Van Lenthe, T. Heine and L. Visscher, *J. Chem. Phys.*, 2016, **144**, 184103.
32 C. A. Ullrich, *Time-dependent density-functional theory: concepts and applications*, OUP Oxford, 2011.
33 M. Marques, A. Rubio, E. K. Gross, K. Burke, F. Nogueira and C. A. Ullrich, *Time-dependent density functional theory*, Springer Science & Business Media, 2006.

34 O. Baseggio, G. Fronzoni and M. Stener, *J. Chem. Phys.*, 2015, **143**, 024106.
35 S. Leseduarte, J. Sellares and A. Travesset, *Surf. Sci.*, 1997, **384**, 1–14.
36 F. Trani, G. Scalmani, G. Zheng, I. Carnimeo, M. J. Frisch and V. Barone, *J. Chem. Theory Comput.*, 2011, **7**, 3304–3313.
37 M. Khodabandeh, N. Asadi-Aghbolaghi and Z. Jamshidi, *J. Phys. Chem. C*, 2019, **123**, 9331–9342.
38 C. Yu, W. Harbich, L. Sementa, L. Ghiringhelli, E. Aprá, M. Stener, A. Fortunelli and H. Brune, *J. Chem. Phys.*, 2017, **147**, 074301.
39 R. Schira and F. Rabilloud, *J. Phys. Chem. C*, 2019, **123**, 6205–6212.
40 C. Yu, R. Schira, H. Brune, B. von Issendorff, F. Rabilloud and W. Harbich, *Nanoscale*, 2018, **10**, 20821–20827.
41 G. Barcaro, M. Broyer, N. Durante, A. Fortunelli and M. Stener, *J. Phys. Chem. C*, 2011, **115**, 24085–24091.
42 M. Stener, A. Nardelli, R. De Francesco and G. Fronzoni, *J. Phys. Chem. C*, 2007, **111**, 11862–11871.
43 C. M. Aikens, S. Li and G. C. Schatz, *J. Phys. Chem. C*, 2008, **112**, 11272–11279.
44 H.-C. Weissker and C. Mottet, *Phys. Rev. B: Condens. Matter Mater. Phys.*, 2011, **84**, 165443.
45 G.-T. Bae and C. M. Aikens, *J. Phys. Chem. C*, 2012, **116**, 10356–10367.
46 X. López-Lozano, H. Barron, C. Mottet and H.-C. Weissker, *Phys. Chem. Chem. Phys.*, 2014, **16**, 1820–1823.
47 G. Barcaro, L. Sementa, A. Fortunelli and M. Stener, *J. Phys. Chem. C*, 2014, **118**, 12450–12458.
48 M. Kuisma, A. Sakko, T. P. Rossi, A. H. Larsen, J. Enkovaara, L. Lehtovaara and T. T. Rantala, *Phys. Rev. B: Condens. Matter Mater. Phys.*, 2015, **91**, 115431.
49 H.-C. Weissker and X. López-Lozano, *Phys. Chem. Chem. Phys.*, 2015, **17**, 28379–28386.
50 O. Baseggio, M. De Vetta, G. Fronzoni, M. Stener, L. Sementa, A. Fortunelli and A. Calzolari, *J. Phys. Chem. C*, 2016, **120**, 12773–12782.
51 P. Koval, F. Marchesin, D. Foerster and D. Sánchez-Portal, *J. Condens. Matter Phys.*, 2016, **28**, 214001.
52 R. Sinha-Roy, P. García-González and H.-C. Weissker, *Nanoscale*, 2020, **12**, 4452–4458.
53 F. Alkan and C. M. Aikens, *J. Phys. Chem. C*, 2018, **122**, 23639–23650.
54 J. Idrobo and S. Pantelides, *Phys. Rev. B: Condens. Matter Mater. Phys.*, 2010, **82**, 085420.
55 N. Asadi-Aghbolaghi, R. Rüger, Z. Jamshidi and L. Visscher, *J. Phys. Chem. C*, 2020, **124**, 7946–7955.
56 G. Giannone and F. Della Sala, *J. Chem. Phys.*, 2020, **153**, 084110.
57 S. D'Agostino, R. Rinaldi, G. Cuniberti and F. Della Sala, *J. Phys. Chem. C*, 2018, **122**, 19756–19766.
58 H.-C. Weissker, O. Lopez-Acevedo, R. Whetten and X. López-Lozano, *J. Phys. Chem. C*, 2015, **119**, 11250–11259.
59 K. Iida, M. Noda and K. Nobusada, *J. Phys. Chem. C*, 2016, **120**, 2753–2759.
60 R. Sinha-Roy, X. López-Lozano, R. L. Whetten and H.-C. Weissker, *Theor. Chem. Acc.*, 2021, **140**, 91–98.
61 E. J. Baerends, *et al.*, ADF2019, SCM, Theoretical Chemistry, Vrije Universiteit, Amsterdam, The Netherlands, https://www.scm.com/, 2019.
62 B. Molina, A. Sánchez-Castillo, S. Knoppe, I. L. Garzón, T. Bürgi and A. Tlahuice-Flores, *Nanoscale*, 2013, **5**, 10956–10962.
63 G. Li, H. Abroshan, C. Liu, S. Zhuo, Z. Li, Y. Xie, H. J. Kim, N. L. Rosi and R. Jin, *ACS Nano*, 2016, **10**, 7998–8005.
64 F. Hidalgo and C. Noguez, *ACS Nano*, 2013, **7**, 513–521.
65 Y. Zheng, W. Liu, T. Lv, M. Luo, H. Hu, P. Lu, S. I. Choi, C. Zhang, J. Tao and Y. Zhu, *Chem. – Asian J.*, 2014, **9**, 2635–2640.
66 Q.-F. Zhang, X. Chen and L.-S. Wang, *Acc. Chem. Res.*, 2018, **51**, 2159–2168.
67 N. Yan, N. Xia, L. Liao, M. Zhu, F. Jin, R. Jin and Z. Wu, *Sci. Adv.*, 2018, **4**, eaat7259–eaat7265.
68 S. H. Vosko, L. Wilk and M. Nusair, *Can. J. Phys.*, 1980, **58**, 1200–1211.
69 E. v. Van Lenthe, J. Snijders and E. Baerends, *J. Chem. Phys.*, 1996, **105**, 6505–6516.
70 R. Van Leeuwen and E. Baerends, *Phys. Rev. A: At., Mol., Opt. Phys.*, 1994, **49**, 2421–2431.
71 E. B. Guidez and C. M. Aikens, *J. Phys. Chem. C*, 2013, **117**, 12325–12336.
72 G. Piccini, R. W. A. Havenith, R. Broer and M. Stener, *J. Phys. Chem. C*, 2013, **117**, 17196–17204.
73 N. Durante, A. Fortunelli, M. Broyer and M. Stener, *J. Phys. Chem. C*, 2011, **115**, 6277–6282.
74 F. Rabilloud, *J. Chem. Phys.*, 2014, **141**, 144302.
75 S. Bernadotte, F. Evers and C. R. Jacob, *J. Phys. Chem. C*, 2013, **117**, 1863–1878.
76 L. Sementa, G. Barcaro, O. Baseggio, M. De Vetta, A. Dass, E. Aprà, M. Stener and A. Fortunelli, *J. Phys. Chem. C*, 2017, 121, 10832–10842.
77 A. Dass, T. Jones, M. Rambukwella, D. Crasto, K. J. Gagnon, L. Sementa, M. De Vetta, O. Baseggio, E. Aprà and M. Stener, *J. Phys. Chem. C*, 2016, **120**, 6256–6261.
78 Q. Shi, Z. Qin, C. Yu, S. Liu, H. Xu and G. Li, *Nanoscale*, 2020, **12**, 4982–4987.
79 A. Tlahuice-Flores, D. M. Black, S. B. Bach, M. Jose-Yacamán and R. L. Whetten, *Phys. Chem. Chem. Phys.*, 2013, **15**, 19191–19195.
80 K. M. Jensen, P. Juhas, M. A. Tofanelli, C. L. Heinecke, G. Vaughan, C. J. Ackerson and S. J. Billinge, *Nat. Commun.*, 2016, **7**, 1–8.
81 S. Malola and H. Häkkinen, *J. Phys. Chem. Lett.*, 2011, **2**, 2316–2321.
82 O. Baseggio, M. De Vetta, G. Fronzoni, M. Stener and A. Fortunelli, *Int. J. Quantum Chem.*, 2016, **116**, 1603–1611.
83 H.-C. Weissker, H. B. Escobar, V. Thanthirige, K. Kwak, D. Lee, G. Ramakrishna, R. Whetten and X. López-Lozano, *Nat. Commun.*, 2014, **5**, 3785–3792.
84 S. Malola, L. Lehtovaara and H. Häkkinen, *J. Phys. Chem. C*, 2014, **118**, 20002–20008.
85 S. Kümmel, *Adv. Energy Mater.*, 2017, **7**, 1700440.
86 J. C. Idrobo, S. Öğüt and J. Jellinek, *Phys. Rev. B: Condens. Matter Mater. Phys.*, 2005, **72**, 085445.
87 R. L. M. Gieseking, A. P. Ashwell, M. A. Ratner and G. C. Schatz, *J. Phys. Chem. C*, 2020, **124**, 3260–3269.

